Wetlands Ecol Manage (2023) 31:435–448
https://doi.org/10.1007/s11273-023-09926-3

ORIGINAL PAPER

Seasonal groundwater salinity dynamics in the mangrove supratidal zones based on shallow groundwater salinity and electrical resistivity imaging data

Joko Prihantono · Takashi Nakamura · Kazuo Nadaoka · Tubagus Solihuddin · Dino Gunawan Pryambodo · Muhammad Ramdhan · Novi Susetyo Adi · Ilham · Anindya Wirasatriya · Sugeng Widada

Received: 22 December 2022 / Accepted: 29 March 2023 / Published online: 10 April 2023
© The Author(s) 2023

Abstract Soil salinity plays an essential role in the growth of mangroves. Mangroves usually grow in intertidal zones. However, in Karimunjawa National Park (KNP), Indonesia, mangroves are also found in supratidal zones. Thus, this study aims to determine why mangroves can grow in this supratidal zone, even during the dry season. We analyze seasonal changes in groundwater flow and salinity dynamics using the hydraulic head, shallow groundwater salinity, and electrical resistivity imaging (ERI) data. The result shows that variation in groundwater salinity is caused by seawater intrusion, which is generated by a hydraulic gradient due to the sea level being higher than the water table in KNP. Rainfall and evapotranspiration, which change seasonally, likely affect the water table fluctuation and salt concentration. ERI images indicate this seawater intrusion in the top sediment up to the bedrock boundary. However, the resistivity difference in the wet and dry seasons shows that remarkable resistivity change occurs at the deeper layer (50–60 m below ground level (BGL)), likely due to freshwater recharge from rainwater on the land side. Groundwater in the KNP is shallow and saline; thus, mangroves in this zone, e.g., *Ceriops tagal* and *Lumnitzera racemosa*, can grow because their roots can reach this groundwater. These mangrove species can still grow in this zone even though the shallow groundwater is very saline (46–50 ppt). However, this condition might cause these mangroves to grow stunted. Thus, freshwater availability is crucial for

J. Prihantono (✉) · T. Nakamura · K. Nadaoka
School of Environment and Society, Tokyo Institute of Technology, Ookayama, Tokyo 152-8552, Japan
e-mail: jk.prihantono@gmail.com

J. Prihantono
Research Center for Concervation of Marine and Inland Water Resources, National Research and Innovation Agency, Cibinong 16911, Indonesia

T. Solihuddin
Research Center for Climate and Atmosphere, National Research and Innovation Agency, Bandung 40173, Indonesia

D. G. Pryambodo
Research Centre for Limnology and Water Resources, National Research and Innovation Agency, Cibinong 16911, Indonesia

M. Ramdhan
Research Center for Geospatial, National Research and Innovation Agency, Cibinong 16911, Indonesia

N. S. Adi · Ilham
Ministry of Marine Affairs and Fisheries, Jakarta 10041, Indonesia

A. Wirasatriya · S. Widada
Department of Oceanography, Faculty of Fisheries and Marine Science, Universitas Diponegoro, Semarang 50275, Indonesia

mangrove growth in this supratidal zone to dilute this high groundwater salinity.

Keywords Mangrove · Groundwater salinity · Electrical resistivity imaging · Seawater intrusion · Supratidal zone · Karimunjawa

Introduction

Soil salinity is essential in mangrove growth and in establishing mangrove ecosystem structures in coastal areas (Ball 2002; Nguyen et al. 2015; Yoshikai et al. 2022). Seawater inundation caused by tides and waves influences soil salinity in coastal areas. Periodic inundation by tides in intertidal areas plays a role in maintaining soil moisture, temperature, and salt dilution (Passioura et al. 1992; Naidoo 2010).

Mangroves grow in saline areas because they adapt better than terrestrial plants (Ball 1988). However, mangroves require fresh water for their growth (Santini et al. 2015; Hayes et al. 2019). Water uptake, transpiration, and photosynthesis in mangroves decrease when groundwater salinity is high (Ball 1988; Parida and Jha 2010; Reef and Lovelock 2015). Consequently, nutrient uptake by mangrove growth is disrupted, leading to mortality (Šimůnek and Hopmans 2009; Dittmann et al. 2022). Limited freshwater supply may occur on small islands because of restricted areas and resources (Falkland 1999). Generally, small islands do not contain rivers that supply freshwater for mangrove growth, such as in Karimunjawa National Park (KNP), Indonesia, where this study was conducted. At these locations, mangroves receive freshwater from rain and groundwater (Prihantono et al. 2021, 2022).

The KNP is a mangrove forest on the coast of a small island. Mangroves in the KNP grow in both intertidal and supratidal zones. The supratidal zone is located above the maximum height of the tide. This zone is not inundated by seawater but may be flooded when the highest tide or storm occurs. Prihantono et al. (2022) suggested that mangroves in intertidal areas grow with taller and greener canopies than those in supratidal zones. In addition, Prihantono et al. (2021) suggested that soil moisture in KNP affects the greenness of mangroves. Soil moisture is influenced by tide inundation, rainwater, and groundwater table. However, they did not discuss the groundwater salinity dynamics in this area which is essential to understand why mangroves can grow here even though they are not waterlogged by tides or rainwater.

Groundwater in coastal areas is saline due to seawater intrusion into the aquifer. Seawater intrusion may occur when sediments in the coastal area have high permeability (Panjaitan et al. 2018), and the groundwater table is lower than the sea level (Jasechko et al. 2020). Therefore, measurement of the hydraulic head at the KNP needs to be performed to determine its position with respect to sea level. Then, the hydraulic gradient of each well can be calculated. In addition, a groundwater flow direction map can be constructed to predict the distribution of shallow groundwater salinity and the seawater intrusion process. Groundwater salinity at the desired depth can be measured directly from water samples using a salinometer or indirectly as electrical resistivity imaging (ERI). ERI is a geophysical method for estimating geological structures and lithology properties using direct current (DC) electricity. One application of the ERI method is to map groundwater salinity and seawater intrusion in coastal areas (Adhikary et al. 2015; Galazoulas et al. 2015; Hermans and Paepen 2020; Folorunso 2021). We can also determine the interseasonal differences in groundwater recharge and salinity using time-lapse ERI (Wagner et al. 2013; Tesfaldet and Puttiwongrak 2019; Mao et al. 2022). In this study, we suspect that mangroves in supratidal zones of the KNP can grow even in different seasons because they are influenced by shallow water tables and saline groundwater due to seawater intrusion.

This study aims to determine the patterns of groundwater salinity, groundwater flow direction, and sediment thickness in the supratidal zones of the KNP in dry and wet seasons using the time series data of hydraulic head, shallow groundwater salinity, and resistivity difference in dry and wet seasons. We also aimed to understand why mangroves can grow in supratidal areas.

Materials and methods

Study site

The study was conducted at KNP on Kemujan Island, Karimunjawa Archipelago, Java Sea, Indonesia

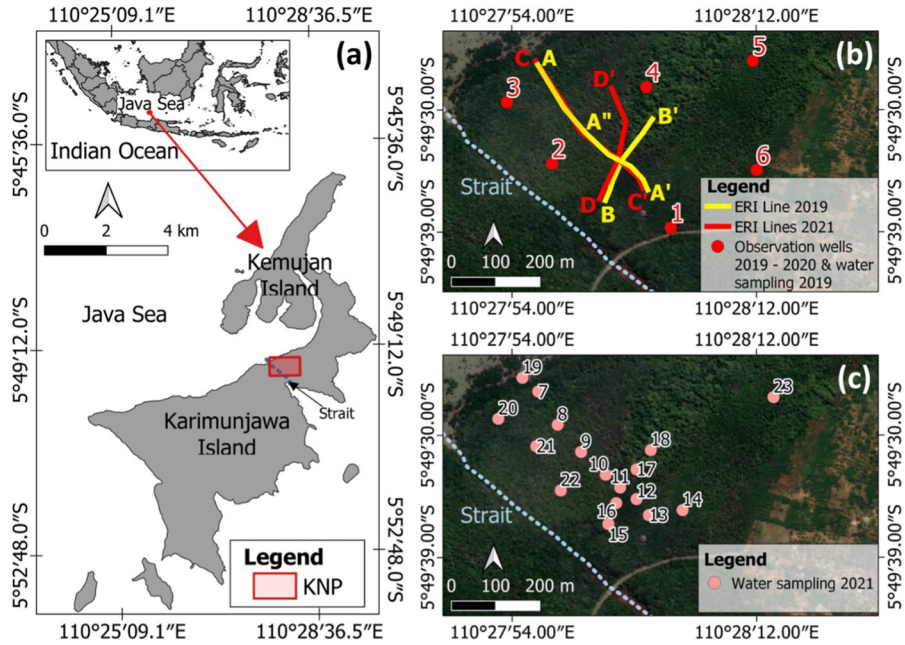


Fig. 1 **a** Location of the Karimunjawa island, separated by a strait from the Kemujan island; **b** ERI measurement locations (yellow, ERI lines in 2019; red, ERI lines in 2021), observation wells in 2019–2020 (red dots) and water sampling location in the dry season of 2019 (red dots); **c** water sampling locations in the wet season of 2021 (pink dots)

(Fig. 1a, 5°49.511′S, 110°28.055′E). This island is north of Karimunjawa Island, separated by a narrow strait. This area has a tropical climate, with an average daily temperature ranging from 26 to 30 °C, an average humidity of 70–85%, and an average annual rainfall of 2,632 mm. The wet season occurs between October and March, and the dry season occurs between April and September, with a monthly average rainfall of 60 mm and 400 mm, respectively (Kamal et al. 2016). The study site is a mangrove forest protected by the Karimunjawa National Park Office (BTNKJ), Ministry of Environment and Forestry of Indonesia, responsible for mangrove conservation, tourism, education, and research. There are at least 13 identified mangrove species, with *Ceriops tagal*, *Rhizophora apiculata*, and *Lumnitzera racemosa* as dominant (Mulyadi et al. 2019). Because KNP is a protected area with small residents in the surrounding area, this study did not consider anthropogenic influences.

The geological map (Sidarto and Hermanto 1993) shows that the Pre-Tertiary island is in the Karimunjawa Formation, consisting of quartz sandstone, micaceous sandstone, quartz conglomerate, quartz siltstone, and quartz shale. The southern part of Kemujan Island contains the Karimunjawa Formation. However, the northern part of Kemujan Island is dominated by the Parang Formation, which contains volcanic breccia, tuff, and lavas from the Tertiary Period. Karimunjawa National Park is geologically located in alluvium from the Quaternary Period and is composed of pebbles, gravel, sand, clay, mud, coral fragments, and pumice. In general, rock formations on Karimunjawa Island show signs of intensive weathering (Hadi et al. 2005), generally resulting in sand and clay. Loose sand is commonly found on flat land. Meanwhile, Kemujan Island is characterized by volcanic rock weathering. Such characteristics cause rainwater to percolate into the Karimunjawa and Kemujan aquifers.

Karimunjawa Island has a high hilly topography, whereas Kemujan Island has a relatively flat topography. On both islands, there is a lowland morphology on the coast generally occupied by mangroves. Only small rivers flow during the wet season and are dry during the dry season. The river follows the valleys of the hills on Karimunjawa Island. Shallow freshwater zones with limited potential and uneven distribution are located in the plains at < 10 m depths (Hadi et al. 2005). Generally, the water quality on both islands is still good and locally used as potable water (Ramdhan et al. 2021).

Hydraulic head calculation and mapping of groundwater flow direction

Hydraulic head monitoring at KNP was carried out in six observation wells (Fig. 1b) from October 11, 2019, to September 29, 2020 at 30 min intervals, based on pressure data obtained from HOBO water level loggers (WLL). Six monitoring wells (30–86 cm) were dug with a hand auger down to the saturated zone; where a PVC pipe with a bottom screen up to 30 cm from the bottom of the casing. A WLL sensor was installed close to the bottom of the well. The geometry of each well (Fig. 2) was documented during the installation and used to calculate the hydraulic head according to Eqs. 1–3.

$$h = hz + hp \tag{1}$$

$$hz = Ground\,Level - \left(L - L_a\right) \tag{2}$$

$$hp = \frac{\left(P_{obs} - P_{atm}\right)}{\rho . g} \tag{3}$$

where h is the hydraulic head or water table from the mean sea level (MSL) (m), hz is the elevation of the WLL sensor from the MSL (m), and hp is the pressure head measured by the WLL sensor (m). The ground level elevation of each well was determined from high-accuracy field measurements of the digital terrain model (DTM) by Wirasatriya et al. (2022) using a geodetic global navigation satellite system (GNSS) in KNP which the elevation of ground level was determined from MSL. L is the total length of the pipe case (m), L_a is the length of the pipe case above ground level (m), P_{obs} is the observed pressure from the sensor (Pa), P_{atm} is the pressure of atmosphere (Pa), ρ is the density of brackish water (kg m^{-3}) = 1011 kg m^{-3}, and g is the acceleration due to gravity (9.8 m s^{-2}). In this study, the pressure of atmosphere (Pa) was obtained from time series atmospheric pressure data of The National Centers for Environmental Prediction-Climate Forecast System Reanalysis (NCEP-CFSR) (Kalnay et al. 1996) from 2019 to 2020.

A groundwater flow direction map was created based on the hydraulic heads obtained from the wells. This map only estimates the flow direction and does not calculate the groundwater speed. It is based only on the hydraulic gradient and does not consider the aquifer's hydraulic properties and geological structures. In this case, we assumed the soil layer was isotropic and homogeneous and only mapped the shallow unconfined aquifer.

We mapped the groundwater flow direction in the dry and wet seasons. The groundwater flow direction in the dry season was determined based on the hydraulic head of all wells on October 28, 2019, at 17:00 UTC, and for the wet season on March 30, 2020, at 17:00 UTC. This map was initiated by interpolating the hydraulic head data using the kriging method in SAGA GIS software version 7.8.2. Then, we determined the flow direction from the obtained contour using SAGA GIS in QGIS software version 3.16.15, using surface gradient tools. The flow direction was orthogonal to the contour lines.

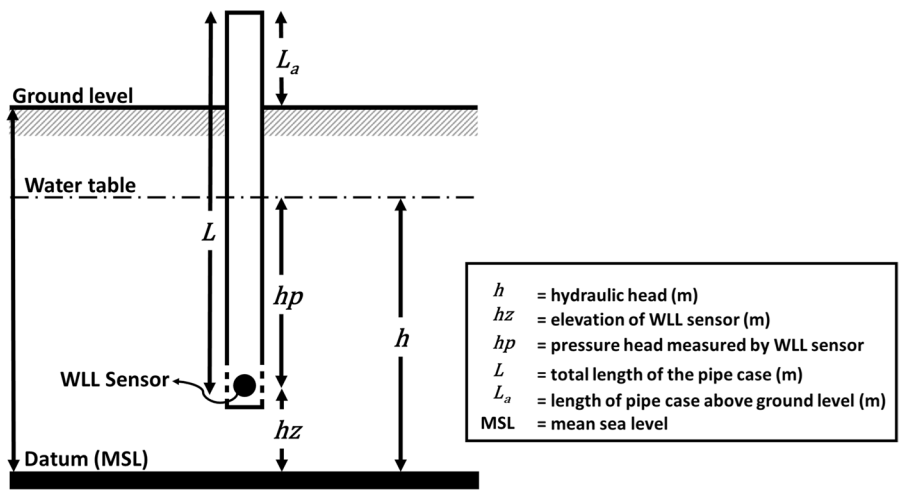


Fig. 2 Sensor installation geometry in observation wells

Shallow groundwater salinity mapping

Salinity maps of the shallow groundwater in the KNP were also done for the dry and wet seasons. Shallow groundwater salinity data during the dry season were obtained from Hudoyo et al. (Hudoyo et al. 2021), with sampling points in six monitoring wells (Fig. 1b) measured with a refractometer. During the wet season, the shallow groundwater salinity was measured using a portable multiparameter water quality meter model WQC-24 (TOA DKK, Japan) in 17 shallows (2–37 cm) holes (Fig. 1c) made with 10 cm wide hand auger. During the wet season, the groundwater table was close (0–17 cm) to the ground level in all the wells. We plotted the salinity values for each season as a map by interpolating the data using the kriging method in the SAGA GIS software version 7.8.2.

Electrical resistivity imaging and calculation of seasonal resistivity difference

We measured three ERI lines during the dry and two during the wet seasons (Fig. 1b). The three ERI lines in the dry season are lines 01, 02, and 03; in the wet season, they are lines 04 and 05. The orientations of lines 01, 02, and 04 are perpendicular to the coastline to the northwest and parallel to the strait to the southwest. Lines 03 and 05 are parallel to the northwest coastline and perpendicular to the strait.

The electrode spacing and total length of each line are shown in Table 1. All ERI lines have identical electrode spacings, except for Line 02, which has an electrode spacing of three meters. Consequently, Line 02 has the shortest total length and the highest resolution among the lines. These ERI lines were measured using a SuperSting Marine electrical resistivity meter (Advance Geoscience, Inc., USA) arranged in a 2D Wenner array.

Table 1 Electrode spacing and total length for electrical resistivity imaging (ERI) lines during the dry and wet seasons of 2019 and 2021, respectively

ERI line	Electrode spacing (m)	Total length (m)	Measurement period
Line 01 (A–A′)	7	385	2019 (Dry season)
Line 02 (A–A″)	3	165	2019 (Dry season)
Line 03 (B–B′)	7	231	2019 (Dry season)
Line 04 (C–C′)	7	385	2021 (Wet season)
Line 05 (D–D′)	7	287	2021 (Wet season)

The measured data were processed to obtain apparent resistivity values. Then we did inverse modeling using Boundless Electrical Resistivity Tomography (BERT) software (Günther et al. 2006) to get the true resistivity value. Generally, BERT inversion is based on a smoothness-constrained Gauss–Newton inversion, as defined by Gunther et al. (Günther et al. 2006). Subsequently, Rucker (2011) detailed the formulation as a flexible minimization and regularization approach. The Gauss–Newton method was used with an inexact line search to solve the inverse issue. Consequently, a solution was reached after a minimum number of iterations.

We used BERT because it is free software and easy to use. It also has the same inversion capabilities as other ERI inversion software (Hellman et al. 2016). We applied the same parameters to all lines in the inversion process. We used a regular or rectangular mesh with 50 layers (LAYERS) and a first layer thickness (PARADZ) equal to the horizontal grid size at the surface (PARADX) of 25% of the electrode spacing. The layer thickness increases linearly with depth. In addition, we applied a vertical constraint (ZWEIGHT) of 0.2, which means that the model was layered. We set other parameters to their default values.

We compared Lines 01 and 04, which had almost the same position, direction, length, and electrode spacing, to determine the resistivity difference between the dry and wet seasons. It wasn't easy to compare other lines due to different electrode positions, directions, lengths, and spacings. The resistivity difference between seasons was determined by subtracting the resistivity of the inversion results in the wet season (2021) from that in the dry season (2019). This can be done because each inversion result has an identical model discretization so that the subtraction process can be performed directly on the same model block.

Bedrock depth estimation

The bedrock depth was estimated by using the Laplacian edge detection (LED) method proposed by Hsu et al. (2010), who used this method to estimate bedrock boundaries in the Peikang River, Central

Taiwan, from the ERI data. We used the following LED equation:

$$\nabla^2\rho(x,z) = \frac{\partial^2\rho}{\partial x^2} + \frac{\partial^2\rho}{\partial z^2} = 0 \quad (4)$$

where ρ is the resistivity in logarithmic scale (Ω m), z is the vertical axis or depth (m) of ρ grid, and x is the horizontal axis (meters) of ρ grid. If LED = 0, there is a drastic change in the resistivity value along the x-axis (horizontal) and depth (vertical). This drastic change indicates the boundary of two main resistivity layers.

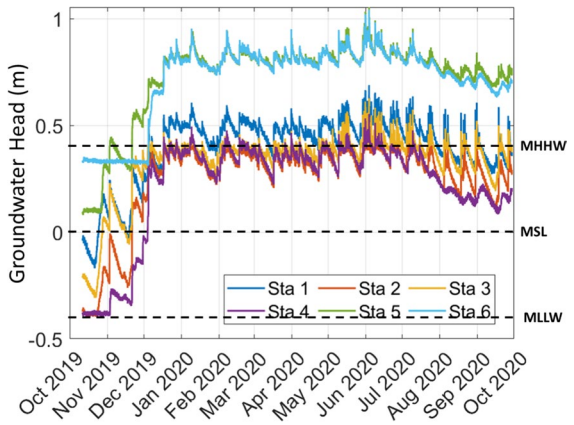


Fig. 3 Hydraulic heads at six observation wells from October 2019 to October 2020 at the supratidal area of KNP. The zero datum refers to the mean sea level.(MSL). The mean higher high water (MHHW) datum is 0.4 m, and the mean lower low water (MLLW) datum is − 0.4 m

Results

Hydraulic head and groundwater flow direction

The hydraulic heads were lower in the dry than in the wet season for all the wells (Fig. 3). The hydraulic heads were at their lowest positions (below MSL) during the October 2019 dry season and increased to the mean value value (close to mean higher high water (MHHW) datum) during the wet season, from December 2019 to July 2020. The mean high higher water (MHHW) in KNP is 0.4 m from MSL, whereas the mean low lower water (MLLW) is -0.4 m from MSL (Prihantono et al. 2022).

When the dry season began at the end of July 2020, the hydraulic heads slowly decreased until October 2020 but were still above MSL. These hydraulic head fluctuations were influenced by recharge from rainfall in KNP and the Kemujan island (Prihantono et al. 2021). Hydraulic heads in the 2019 dry season were lower than those in the 2020 dry season because rainfall in the 2019 dry season was lower than in the 2020 dry season due to the eastern monsoon (El Niño), and a positive Indian Ocean Dipole (IOD) (Prihantono et al. 2021, 2022; Ramadhan et al. 2021).

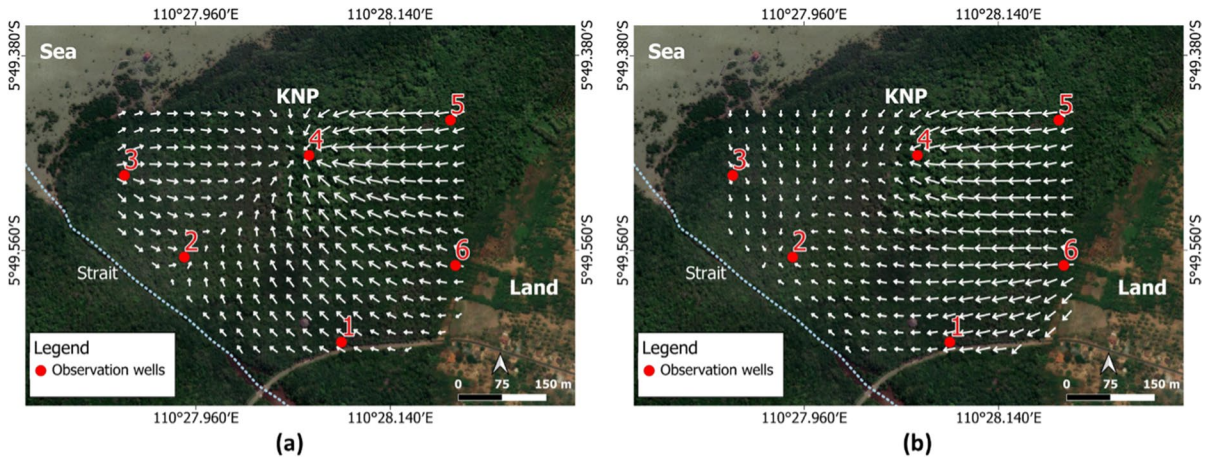


Fig. 4 Groundwater flow direction in (**a**) the 2019 dry season, and (**b**) 2020 wet season in KNP. The arrow size indicates the magnitude of the hydraulic gradient

The map of groundwater flow direction in the dry season of 2019 (Fig. 4a) shows that groundwater flows from the coast and landsides to the middle area of the KNP (Station 4). On the other hand, the groundwater flow direction map in the wet season of 2020 (Fig. 4b) shows groundwater flowing from the land side and the northern coastline moving towards the middle area and turning towards the strait (Station 2).

Shallow groundwater salinity in different seasons

The salinity of the shallow groundwater in the observation wells in the 2019 dry season ranged from 46 to 50 ppt (Fig. 5a), indicating that shallow groundwater salinity in the 2019 dry season was higher in KNP than that of the surrounding seawater, which ranged from 27 to 33 ppt (Marine Research Center 2019). The 2019 dry season was extremely arid because rainfall was lower than average. Also, the shallow groundwater salinity in the middle area of the KNP (Stations 4 and 5) was higher than landward and toward the coastline (Fig. 5a). In contrast, shallow groundwater salinity during the wet season of 2021 ranged from 0 to 27 ppt (Fig. 5b) and was lower in the landward zone than in the coastline.

Subsurface resistivity interpretation

The inversion results of all ERI lines show small root mean square (RMS) and relative root mean square (RRMS) errors with a range of 0.06–0.112 Ω m and 2.138–9.943%, respectively. These small error values indicate that the obtained resistivity models have good statistical quality and that the ERI images can be used to explore subsurface conditions in KNP. The maximum depth of ERI images in the dry season was 60 m, whereas in the wet season was 40 m. The resistivity results range from 0.17–18.07 Ω m. Generally, the ERI images in the dry (Figs. 6a, c) and wet (Figs. 6b, d) seasons showed a similar pattern. There was a lower resistivity in upper layer than in the lower layer, indicating that the upper layer is more saline than the deeper layer.

Based on the resistivities of common rocks and minerals table compiled by Glover (2015), the salinity of groundwater in the KNP is classified into three parts by assuming that the soil is water-saturated. The top layer (0–10 m) has a resistivity of 0.17–1 Ω m and is categorized as brine water. The middle layer (10–50 m) has a resistivity of 1–10 Ω m, indicating brackish water. The 50–60 m deep layer is more likely to contain fresh water because it has a 10–18 Ω m resistivity.

Horizontally, the ERI images parallel to the strait (Line 01, Fig. 6a; Line 03, Fig. 6b) show the low resistivity (0.17–4.14 Ω m) on landward is thicker

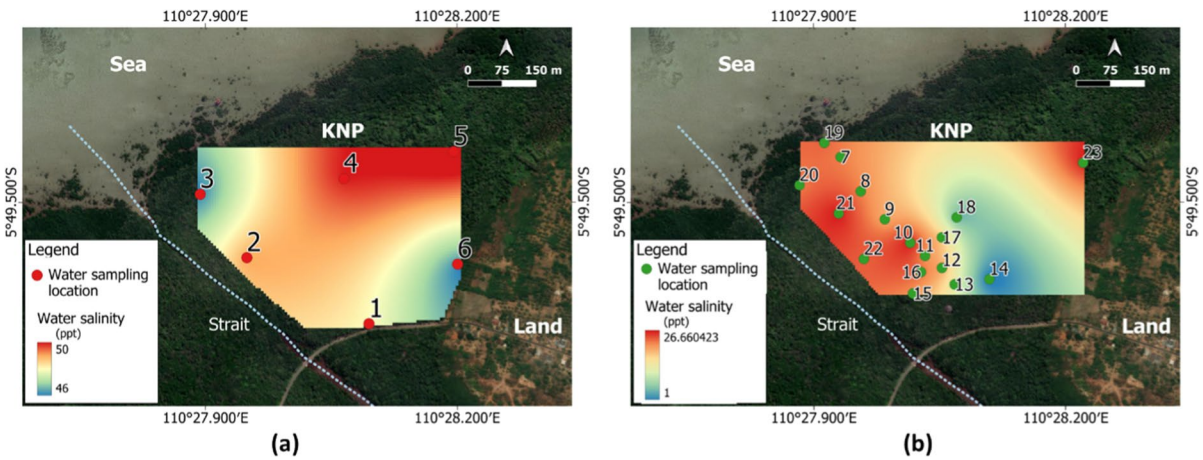


Fig. 5 Shallow groundwater salinity in the KNP during (**a**) the dry season of 2019 and (**b**) the wet season of 2021. Groundwater salinity in the dry season of 2019 was higher than in the wet season of 2021. During the dry season, groundwater salinity in the middle of KNP was the highest, and it became lower than surrounding during the wet season

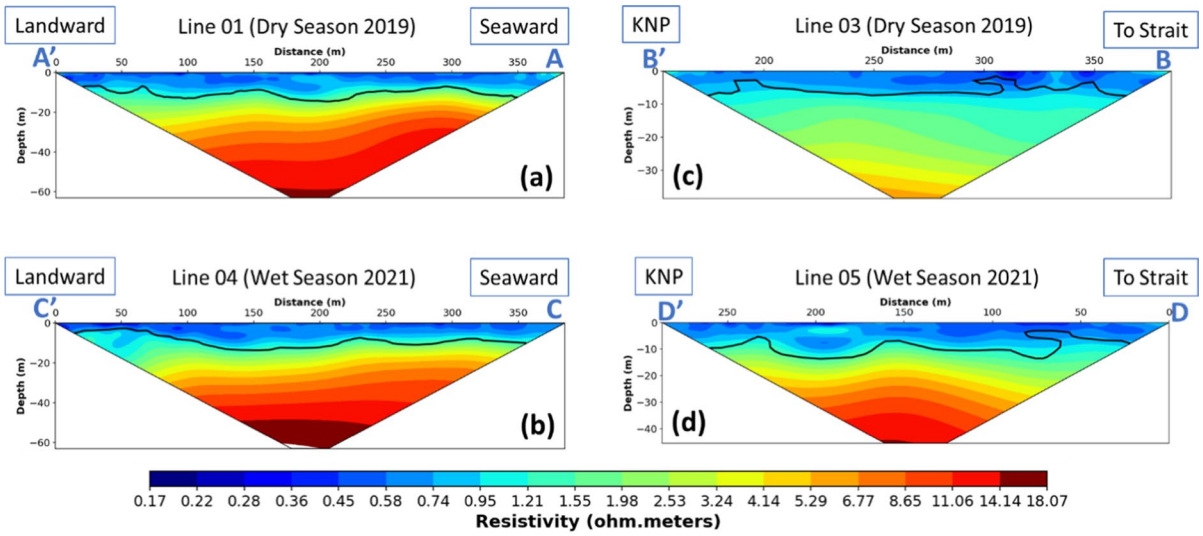


Fig. 6 ERI images of lines 01 (**a**), 02 (**b**), 03 (**c**), and 04 (**d**). Black contour lines represent the bedrock boundary

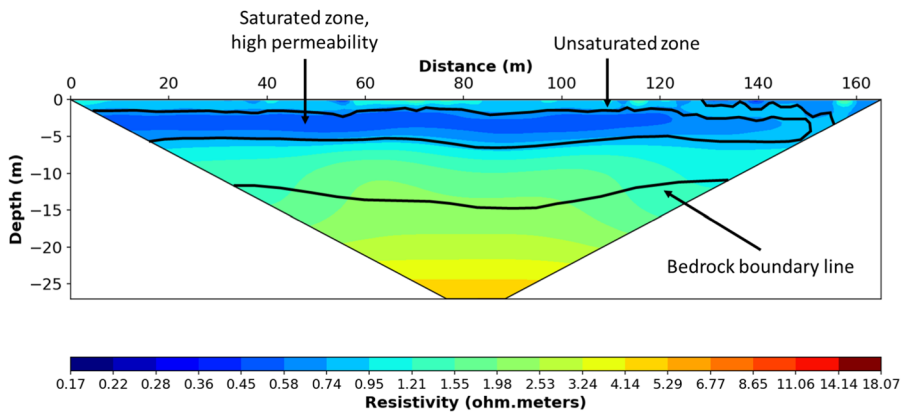


Fig. 7 ERI image of Line 02 with the resistivity boundary lines (black lines) obtained from the LED method. The black lines denote the boundary of the saturated–unsaturated zone (2–3 m BGL), the edge of the high-low permeable zone (5–8 m BGL), and the bedrock boundary (10–15 m BGL)

than seaward. Moreover, the ERI images perpendicular to the strait (Line 02, Fig. 6c; Line 04, Fig. 6d) show low resistivity on the strait area is thicker than in the middle area of the KNP. The thicker layer of lower resistivities suggests the influence of seawater from the strait is considerable in these ERI lines.

The maximum depth of the ERI image of Line 02 (Fig. 7) was 26 m. It shows that the resistivity of the top layer was lower than that of the deeper layer. The resistivity in the 0–10-m layer ranges from 0.45 to 2 Ω m, and the 10–26-m layer ranges from 2 to 5 Ω m. These resistivities slightly differ from Line 01 (Fig. 6a) at the same location at 0–10 m layer; they range from 0.45 to 1 Ω m to 1–8.6 Ωm at 10–26-m depths. Generally, the resistivity pattern of Line 02 with Line 01 is similar. But Line 02 can depict in detail the resistivity.

The ERI image of Line 02, the unsaturated zone was clearly delineated at the top layer (0–2 m) because this resistivity (0.74–1.21 Ω m) is higher than beneath it. This layer was confirmed with the water table depth from the nearest wells (stations 3 and 2), which ranges from 0.48 to 0.73 m below ground level (BGL). Moreover, the lower layer (2–8 m) shows the lowest resistivity (0.45–0.95 Ω m), which seawater may fill due to high permeability. In the 8–27-m depth, the resistivity ranges from 0.95 to 5.29 Ω m, which is interpreted as a saturated zone with brackish groundwater due to the mixing

of seawater from the upper layer with fresh water from the deep aquifer.

The bedrock depth in all ERI images obtained using the LED method ranged from 10 to 15 m (BGL, black contour lines, Figs. 6, 7), corresponding to the sediment thickness above the bedrock, which coincides with the resistivity of 0.95–1.21 Ω m for all ERI lines except for Line 02. The bedrock boundary in Line 02 was on the resistivity of 1.21–1.98 Ω m. Moreover, on Line 02, the LED method can delineate the edge of the saturated and unsaturated zone at a depth of 2–3 m BGL. In addition, this method also traces the boundary of the high-low permeable zone in Line 02 at a depth of 5–8 m BGL.

Resistivity difference between dry and wet season

In the dry (Line 01) and wet (Line 03) season at KNP the resistivity difference range is – 4–4 Ω m (Fig. 8a), with dominant values ranging from − 0.2–0.2 Ω m (see also Fig. 8b). The mean and standard deviation of the resistivity differences were − 0.015 and 0.75, respectively. Similarly, the relative resistivity difference percentage to the 2019 resistivity (Fig. 8c) shows values ranging from − 60 to 120%. However, the dominant value is approximately – 20–20%. The percentage value of more than 100% is minimal. Thus, these results suggest that the resistivity difference between the 2021 wet and 2019 dry seasons was relatively small. Significant changes were observed in the small areas.

A negative resistivity difference indicates a decrease in resistivity, which means that the resistivity of the 2021 wet season is lower than that of the 2019 dry season. Conversely, positive resistivity shows an increase in resistivity, which means that the resistivity of the 2021 wet season is higher than the 2019 dry season. Because resistivity is inversely proportional to salinity, an increase in resistivity

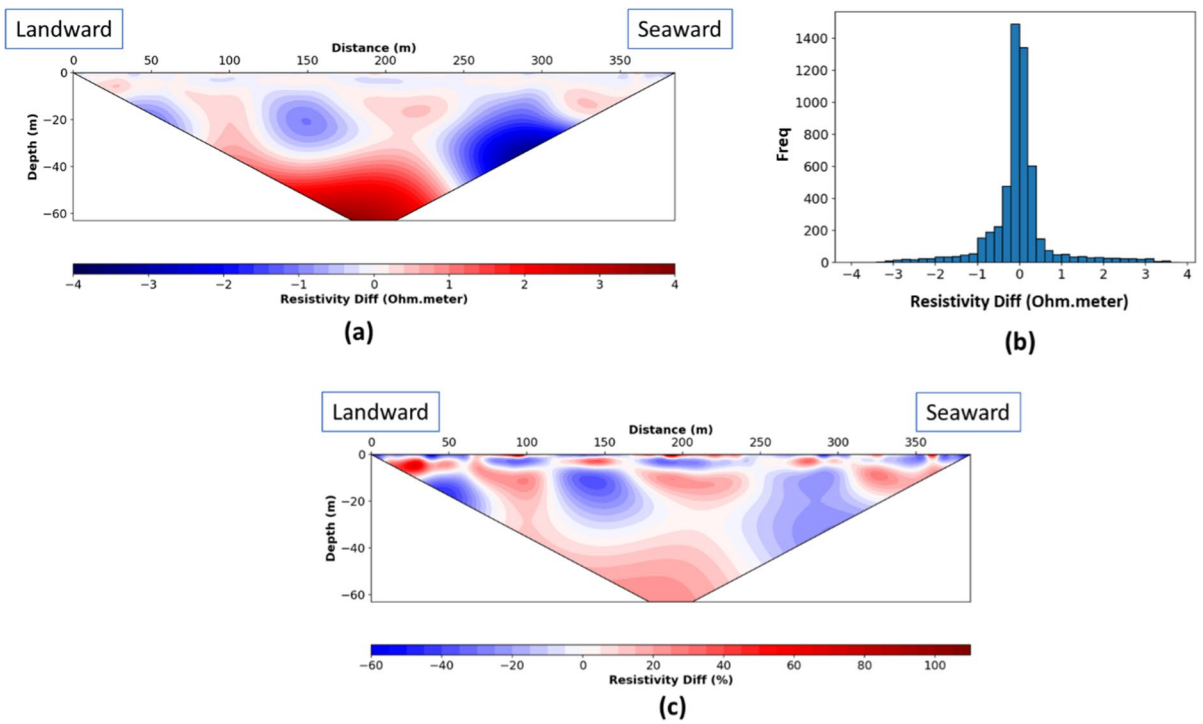


Fig. 8 **a** The cross-sectional image shows the absolute value of resistivity difference in the dry season 2019 (Line 01) and wet season 2021 (Line 03) at KNP. **b** Histogram shows the dominant value of this absolute resistivity difference (− 0.2–0.2 Ω m). **c** The cross-section image shows the relative resistivity difference to the dry season of 2019. The cross-section images and the histogram show a small value in resistivity difference. However, these cross-sections indicate a continuous pattern of high resistivity difference from the deep layer to the middle layer suggesting freshwater from the deep layer emerges to the middle layer

indicates a decrease in salinity; conversely, a decrease in resistivity indicates an increase in salinity.

Some areas in the upper layer (0–10 m) experienced increased or decreased resistivity, probably related to the relative contribution of rainfall recharge and seawater intrusion, respectively. The average increase and decrease in the resistivity of this layer ranged from − 40 to 40%, which is considered a small difference. Therefore, the salinity in the 2021 wet season was similar to that in the 2019 dry season in this layer. However, some areas on the surface at a distance of approximately 190 m experienced an increase in resistivity of 120%.

There was a relatively small resistivity difference at the middle depth (10–50 m) with a range of − 40–40% from the 2019 dry season. This difference suggests that the groundwater salinity in the wet season was relatively similar to that in the 2019 dry season. At depth of 50–60 m, it only showed an increase in resistivity and did not show a decrease in resistivity. This increase in resistivity reached 25% from the 2019 dry season. It means that the salinity of groundwater in the 2021 wet season was relatively similar to that in the 2019 dry season, and the quantity has increased from the 2019 dry season conditions. The continuous pattern of high resistivity difference from the deep layer to the middle layer indicates freshwater from the deep layer emerges to the middle layer.

Discussion

The WLL data in this study had a relatively high resolution with a sampling time of 30 min. With this resolution, water table changes can be recorded. However, the hydrograph at wells 2, 4, 5, and 6 in October 2019 (Fig. 3) appeared relatively flat. These water tables might be at a lower depth than the sensor's level. Thus, the water pressure could not be measured. Nevertheless, the water table was close to the sensor because Hudoyo et al. (Hudoyo et al. 2021) successfully measured the salinity of shallow groundwater in October 2019 by sampling the water directly in these wells. Therefore, these data can be used to analyze the groundwater dynamics in the study area by assuming that the hydraulic head is equal to the elevation of the sensor.

Shallow groundwater flow direction and salinity map indicate seawater intrusion in KNP. In the dry season of 2019, the arrows of groundwater flow from the coast toward the middle of the KNP area are more remarkable than during the wet season of 2020, suggesting that seawater intrusion is more prominent during the dry season than during the wet season. This is because the water table in the center of the KNP (Station 4) was in the lowest condition, and almost all the water tables were below the MSL. However, these groundwater heads were above MSL during the dry season of 2020 (July to September). Still, this hydraulic head shows a similar pattern to the hydraulic head during the dry season of 2019. Therefore, the groundwater flow direction during the dry season of 2020 and 2019 might be equal, and strong seawater intrusion may still occur due to its position below MHHW. This means the water table is lower than the seawater level despite decreasing hydraulic gradient.

During the wet season, the water table in the middle area of the KNP rises, and some of the water tables in the strait become the lowest. Thus, the groundwater flowed to some regions in the strait. The groundwater flow direction from the land towards the middle of the KNP during the wet season suggests the presence of fresh groundwater from the land flowing into the middle of the KNP area, which mixed with saline water from seaward and became brackish. During the dry season, groundwater flow from the land toward the middle of KNP was less prominent than seawater intrusion from the seaward and strait.

Climatic factors, such as rainfall and temperature, significantly influence groundwater levels and salinity. This agrees with the study by Yan et al. (Yan et al. 2015), who used almost the same method by measuring groundwater level and salinity in the coastal plain region of Jiangsu Province, China. The groundwater level and salinity were associated with the season. During the dry season, the water table will decline, and groundwater salinity will become high because of low recharge and high evapotranspiration rate due to increasing temperature, thus generating seawater intrusion and salt accumulation near the root zones (Wang et al. 2022). This condition might cause the groundwater salinity in the middle area of KNP to be higher than the surrounding seawater during the dry season of 2019, which was extreme of the dry season. During the wet season, the water table rises, and groundwater salinity decreases because of

high recharge, low evapotranspiration rate, and fresh groundwater flow from inland, thus causing salt dilution in the soil.

ERI images indicate seawater intrusion in the top layer (0–10 m), brackish water in the middle layer (10–50 m), and fresh water in the deep layer (50–60 m). The brackish water in the middle layer is due to a mixing of saline water from the top layer and fresh water from the deep layer. Based on the ERI image difference in the wet and dry seasons, the groundwater salinity at a depth of more than one-meter BGL suggested small seasonal salinity changes. However, the pattern indicates fresh water from the deep layer rises and mixes with saline water in the middle layers during the wet season. The increased amount of freshwater in the deep layer likely indicates recharging from the mainland. Therefore, significant groundwater salinity changes are likely to occur only in shallow groundwater with a thickness of about 0.25–1-m BGL and at the deeper layer (50–60 m BGL). The groundwater and salinity dynamics of KNP can be illustrated in Fig. 9.

Based on the ERI images, the top layer up to the bedrock boundary (10–15 m BGL) are sediments considered permeable alluvial layers; therefore, seawater easily intrudes into this layer (Costall et al. 2020; Prusty and Farooq 2020). We suspect this layer was a shallow coastal area occupied by mangroves. Then, mangroves in this area act as sediment traps (Hongwiset et al. 2022), and the sedimentation becomes more massive. Consequently, the Karimunjawa Strait narrows due to sedimentation and mangrove growth. The narrowing of the Karimunjawa Strait can be seen in a remote sensing study by Latifah et al. (Latifah et al. 2018). Moreover, ERI images indicate this sedimentation to the strait direction by the thicker lowest resistivity near the strait area. This hypothesis allows the presence of remnants of salt (Meyer et al. 2019) in KNP from the past, which causes groundwater to be saline, and salt dilution only occurs at the surface layer.

Mangroves can grow in the supratidal areas of the KNP because the groundwater is shallow and saline. Thus, mangroves can take up water and nutrients for growth (Selker et al. 1999; Tindall et al. 1999). Moreover, *Ceriops tagal* and *Lumnitzera racemosa*, the dominant mangroves species in this area, can grow in areas with high soil salinity (28–35 ppt) conditions and do not require flooding or less moist soil (Patel et al. 2010; Lyn Estomata and Abit 2011; Perera et al. 2013). However, in this study, these mangrove species could grow in shallow groundwater with a high salinity range of 46–50 ppt. Although, these mangroves tend to grow stunted because of the high salinity of

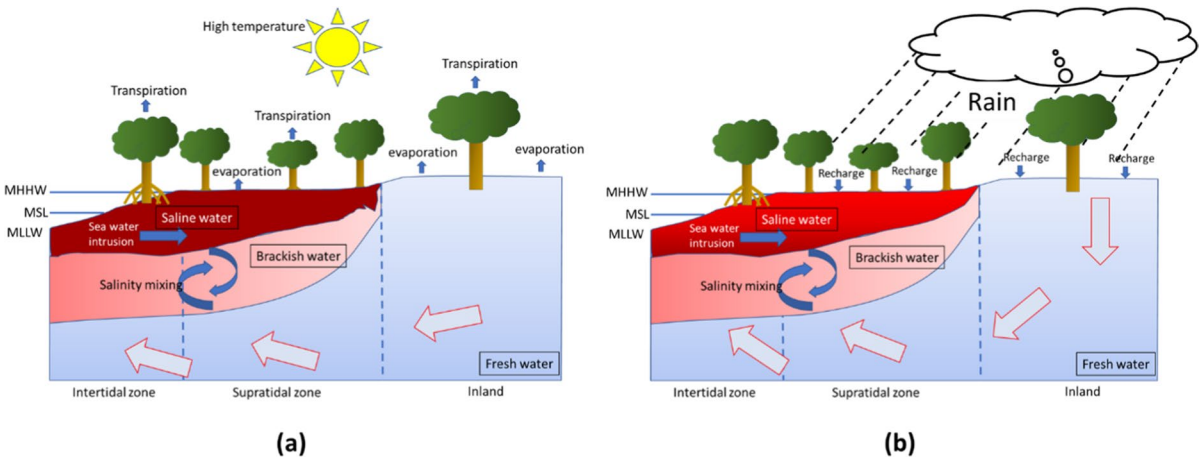


Fig. 9 Illustration image of groundwater flow and salinity dynamic in KNP (**a**) during the dry season and (**b**) during the wet season. **a** During the dry season, shallow groundwater salinity in the top layer is high due to evapotranspiration. In the middle layer, freshwater from the deeper layer mix with saline water from the top layer. **b** During the wet season, seawater intrusion in the top layer and salinity mixing in the middle layer still occur, but the salinity reduces because freshwater recharge dilutes the salt in the shallow groundwater in the supratidal zone and the amount of freshwater from the deeper layer increase. However, this salinity change is not much different except in shallow groundwater (0–1 m BGL)

shallow groundwater. Moreover, fresh groundwater supply is more available during the wet season (Prihantono et al. 2022). Therefore, groundwater preservation by society in Karimunjawa and Kemujan islands is necessary for mangrove conservation in KNP. This groundwater preservation can be applied by avoiding overpumping groundwater and constructing recharge wells. In addition, the government should regulate groundwater utilization and construct retention basins to collect fresh water to serve potable water for society in Karimunjawa.

Conclusions

Groundwater flow and salinity dynamics in the supratidal zone in KNP change with seasons. During the dry season, groundwater salinity is higher than in the wet season due to seawater intrusion caused by prominent hydraulic gradients. This hydraulic gradient occurs because the sea level is higher than the water table in the supratidal zone. This water table change is affected by rainfall and evapotranspiration. Rainfall also contributes to salt dilution in the soil, whereas evapotranspiration contributes to salt accumulation in soil and mangrove root. ERI images indicate seawater intrusion in the top layer up to the bedrock boundary (10–15 m BGL), considered permeable sediment.

Based on the analysis of resistivity difference in the wet and dry seasons, the remarkable resistivity change occurs at the surface layer (0–1 m BGL) and the deeper layer (50–60 m BGL). At the top layer, the resistivity change is influenced by the percolation of freshwater from rainwater. In addition, fresh groundwater flows from the land side to the deeper layer during the wet season. This fresh groundwater in the deeper layer flow to the middle layer and mix with the saline water from the top layer.

Mangroves in the supratidal zone of KNP can grow even during the dry season because the groundwater in this area is shallow and saline. Therefore, the mangrove's roots can reach this groundwater. Dominant mangrove species in this supratidal zone, e.g. *Ceriops tagal*, and *Lumnitzera racemosa*, can still grow even though shallow groundwater salinity was 46–50 ppt. However, this condition might cause these mangroves to grow stunted. Thus, the freshwater availability is crucial for mangrove growth in this supratidal zone. Therefore, groundwater preservation in Karimunjawa island and Kemujjan island is necessary for mangrove conservation in KNP.

Acknowledgements We thank JICA-JST-KKP for funding the ERI survey and groundwater level observations from 2019 to 2020 through the BlueCARES SATREPS project. We also thank the Marine Research Center, Ministry of Marine Affairs and Fisheries of Indonesia (KKP), for funding the ERI and groundwater salinity survey in 2021. We also thank Dr. Semeidi Husrin and Nia Naelul Hasanah, M.Soc.Sc, Head of the Research Institute for Coastal Resources and Vulnerability (LRSDKP), KKP, Bungus, for providing recommendations and permits for the use of ERI instruments of LRSDKP in the 2021 survey. We also thank the University Diponegoro team, who assisted in collecting groundwater level data for 2019–2020, and Vivi Yovita, Sofyan Muji, and Peter Mangindaan, who assisted in collecting the data for 2021.

Author contributions JP, TN, KN, and TS contributed to the conception, design, and analysis of the study. DGN, MR, I, NSA, AW, and SW performed material preparation and data collection. JP wrote the first draft of the manuscript, and all authors contributed to the discussion and commented on previous versions. All authors read and approved the final manuscript.

Funding This work was supported by Japan Science and Technology Agency (JST)–Japan International Cooperation Agency (JICA)–Ministry of Marine Affairs and Fisheries (MAF) of Republic Indonesia for the ERI survey and groundwater level observations from 2019 to 2020 through the BlueCARES SATREPS project. This work also was supported by Marine Research Center (MRC), MAF for the ERI and groundwater salinity survey in 2021.

Data availability The datasets generated during and/or analysed during the current study are available from the corresponding author on reasonable request.

Declarations

Competing interests The authors have no relevant financial or non-financial interests to disclose.

Open Access This article is licensed under a Creative Commons Attribution 4.0 International License, which permits use, sharing, adaptation, distribution and reproduction in any medium or format, as long as you give appropriate credit to the original author(s) and the source, provide a link to the Creative Commons licence, and indicate if changes were made. The images or other third party material in this article are included in the article's Creative Commons licence, unless indicated otherwise in a credit line to the material. If material is not included in the article's Creative Commons licence and your intended use is not permitted by statutory regulation or exceeds the permitted use, you will need to obtain permission directly

from the copyright holder. To view a copy of this licence, visit http://creativecommons.org/licenses/by/4.0/.

References

Adhikary PP, Chandrasekharan H, Dubey SK et al (2015) Electrical resistivity tomography for assessment of groundwater salinity in west Delhi, India. Arab J Geosci 8:2687–2698. https://doi.org/10.1007/s12517-014-1406-y

Ball MC (1988) Ecophysiology of mangroves. Trees 2:129–142. https://doi.org/10.1007/BF00196018

Ball MC (2002) Interactive effects of salinity and irradiance on growth: implications for mangrove forest structure along salinity gradients. Trees - Struct Funct 16:126–139. https://doi.org/10.1007/s00468-002-0169-3

Costall AR, Harris BD, Teo B et al (2020) Groundwater throughflow and seawater intrusion in high quality coastal aquifers. Sci Rep 10:1–33. https://doi.org/10.1038/s41598-020-66516-6

Dittmann S, Mosley L, Stangoulis J et al (2022) Effects of extreme salinity stress on a temperate mangrove ecosystem. Front for Glob Chang 5(859283):1–18. https://doi.org/10.3389/ffgc.2022.859283

Falkland T (1999) Water resources issues of small island developing states. Nat Resour Forum 23:245–260. https://doi.org/10.1111/J.1477-8947.1999.TB00913.X

Folorunso AF (2021) Mapping a spatial salinity flow from seawater to groundwater using electrical resistivity topography techniques. Sci Afr. https://doi.org/10.1016/J.SCIAF.2021.E00957

Galazoulas EC, Mertzanides YC, Petalas CP et al (2015) Large scale electrical resistivity tomography survey correlated to hydrogeological data for mapping groundwater salinization: a case study from a multilayered coastal aquifer in rhodope, Northeastern Greece. Environ Process 2:19–35. https://doi.org/10.1007/s40710-015-0061-y

Glover PWJ (2015) Geophysical Properties of the Near Surface Earth: Electrical Properties. Treatise on Geophysics, 2nd edn. Elsevier, Amsterdam, pp 89–137

Günther T, Rücker C, Spitzer K (2006) Three-dimensional modelling and inversion of dc resistivity data incorporating topography – II. Invers Geophys J Int 166:506–517. https://doi.org/10.1111/J.1365-246X.2006.03011.X

Hadi IS, Arsadi EM, Tjiptasmara (2005) Preliminary Study of Freshwater Resources Karimunjawa-Kemujan Island. Limnotek XII:1–15

Hayes MA, Jesse A, Welti N et al (2019) Groundwater enhances above-ground growth in mangroves. J Ecol 107:1120–1128. https://doi.org/10.1111/1365-2745.13105

Hellman K, Johansson SJ, Olsson PO, Dahlin TD (2016) Resistivity inversion software comparison. In: 22nd European Meeting of Environmental and Engineering Geophysics, Near Surface Geoscience 2016. European Association of Geoscientists & Engineers, Barcelona, Spain, pp 1–5

Hermans T, Paepen M (2020) Combined Inversion of land and marine electrical resistivity tomography for submarine groundwater discharge and saltwater intrusion characterization. Geophys Res Lett. https://doi.org/10.1029/2019GL085877

Hongwiset S, Rodtassana C, Poungparn S et al (2022) Synergetic roles of mangrove vegetation on sediment accretion in coastal mangrove plantations in central Thailand. Forests. https://doi.org/10.3390/F13101739

Hsu HL, Yanites BJ, Chen C chih, Chen YG (2010) Bedrock detection using 2D electrical resistivity imaging along the Peikang River, central Taiwan. Geomorphology 114:406–414. https://doi.org/10.1016/j.geomorph.2009.08.004

Hudoyo F, Widada S, Maslukah L et al (2021) Study of tidal analysis distribution of brackish groundwater and sediments and their effect on mangrove distribution patterns in the Karimunjawa Islands. Indones J Oceanogr. https://doi.org/10.14710/ijoce.v3i4.12916

Jasechko S, Perrone D, Seybold H et al (2020) Groundwater level observations in 250,000 coastal US wells reveal scope of potential seawater intrusion. Nat Commun 11:3229. https://doi.org/10.1038/s41467-020-17038-2

Kalnay E, Kanamitsu M, Kistler R et al (1996) The NCEP/NCAR 40-year reanalysis project. Bull Am Meteorol Soc 77:437–472. https://doi.org/10.1175/1520-0477(1996)077%3c0437:TNYRP%3e2.0.CO;2

Kamal M, Hartono H, Wicaksono P et al (2016) Assessment of mangrove forest degradation through canopy fractional cover in Karimunjawa Island. Cent Java, Indones, Geoplanning J Geomat Plan. https://doi.org/10.14710/geoplanning.3.2.107-116

Latifah N, Febrianto S, Endrawati H, Zainuri M (2018) Mapping of classification and analysis of changes in mangrove ecosystem using multi-temporal satellite images in Karimunjawa Jepara, Indonesia. J Kelaut Trop. https://doi.org/10.14710/jkt.v21i2.2977

Lyn Estomata NB, Abit PP (2011) Growth and survival of mangrove seedlings under different levels of salinity and drought stress. Ann Trop Res 33:107–129. https://doi.org/10.32945/atr3326.2011

Mao D, Wang X, Meng J et al (2022) Infiltration assessments on top of yungang grottoes by time-lapse electrical resistivity tomography. Hydrology. https://doi.org/10.3390/hydrology9050077

Marine Research Center (2019) Annual Report: Study of Ecosystem Service and Blue Carbon Ecosystem Conservation. Location: Karimunjawa. Jakarta

Meyer R, Engesgaard P, Sonnenborg TO (2019) Origin and dynamics of saltwater intrusion in a regional aquifer: combining 3-d saltwater modeling with geophysical and geochemical data. Water Resour Res 55:1792–1813. https://doi.org/10.1029/2018WR023624

Mulyadi, Susanto H, Devi Y, Sahwan FF (2019) Interpretation of Mangrove Trekking Karimunjawa National Park, Second edi. Karimunjawa National Park Office (BTNKJ), Semarang

Naidoo G (2010) Ecophysiological differences between fringe and dwarf Avicennia marina mangroves. Trees - Struct Funct 24:667–673. https://doi.org/10.1007/s00468-010-0436-7

Nguyen HT, Stanton DE, Schmitz N et al (2015) Growth responses of the mangrove Avicennia marina to salinity: development and function of shoot hydraulic systems

require saline conditions. Ann Bot 115:397–407. https://doi.org/10.1093/aob/mcu257
Panjaitan D, Tarigan J, Rauf A, Nababan ESM (2018) Determining sea water intrusion in shallow aquifer using Chloride Bicarbonate Ratio Method. IOP Conf Ser Earth Environ Sci 205:12029. https://doi.org/10.1088/1755-1315/205/1/012029
Parida AK, Jha B (2010) Salt tolerance mechanisms in mangroves: a review. Trees - Struct Funct 24:199–217. https://doi.org/10.1007/s00468-010-0417-x
Passioura JB, Ball MC, Knight JH (1992) Mangroves may salinize the soil and in so doing limit their transpiration rate. Funct Ecol 6:476. https://doi.org/10.2307/2389286
Patel NT, Gupta A, Pandey AN (2010) Strong positive growth responses to salinity by Ceriops tagal, a commonly occurring mangrove of the Gujarat coast of India. AoB Plants 2010:11. https://doi.org/10.1093/AOBPLA/PLQ011
Perera KARS, Amarasinghe MD, Somaratna S (2013) Vegetation Structure and species distribution of mangroves along a soil salinity gradient in a micro tidal estuary on the north-western coast of Sri Lanka. Am J Mar Sci. https://doi.org/10.12691/MARINE-1-1-2
Prihantono J, Adi NS, Nakamura T, Nadaoka K (2021) The impact of groundwater variability on mangrove greenness in Karimunjawa National Park based on remote sensing study. IOP Conf Ser Earth Environ Sci. https://doi.org/10.1088/1755-1315/925/1/012064
Prihantono J, Nakamura T, Nadaoka K et al (2022) Rainfall variability and tidal inundation influences on mangrove greenness in Karimunjawa National Park, Indonesia. Sustainability 14:1–18. https://doi.org/10.3390/su14148948
Prusty P, Farooq SH (2020) Seawater intrusion in the coastal aquifers of India—A review. HydroResearch 3:61–74. https://doi.org/10.1016/j.hydres.2020.06.001
Ramadhan F, Kunarso K, Wirasatriya A et al (2021) Differences in depth and thickness of the thermocline layer on ENSO IOD and monsoon variability in Southern Java Waters. Indones J Oceanogr 3:214–223. https://doi.org/10.14710/ijoce.v3i2.11392
Ramdhan M, Priyambodo DG, Yulius, et al (2021) Study of Utilization of Surface Water Resources on Karimunjawa Island and Kemujan Island. In: Prosiding Seminar Nasional Hari Air Dunia. Palembang, pp 10–15
Reef R, Lovelock CE (2015) Regulation of water balance in mangroves. Ann Bot 115:385–395. https://doi.org/10.1093/aob/mcu174
Rücker C (2011) Advanced Electrical Resistivity Modelling and Inversion using Unstructured Discretization. University of Leipzig
Santini NS, Reef R, Lockington DA, Lovelock CE (2015) The use of fresh and saline water sources by the mangrove Avicennia marina. Hydrobiologia 745:59–68. https://doi.org/10.1007/s10750-014-2091-2
Selker JS, Keller CK, McCord JT (1999) An introduction to the vadose zone. Vadose Zo Process CRC Press LLC Boca Raton, FL, USA 3–20
Sidarto SS, Hermanto B (1993) Geological Map of The Karimunjawa Sheet. Jawa Scale 1(100):000
Šimůnek J, Hopmans JW (2009) Modeling compensated root water and nutrient uptake. Ecol Modell 220:505–521. https://doi.org/10.1016/J.ECOLMODEL.2008.11.004
Tesfaldet YT, Puttiwongrak A (2019) Seasonal groundwater recharge characterization using time-lapse electrical resistivity tomography in the Thepkasattri watershed on Phuket Island. Thailand. https://doi.org/10.3390/hydrology6020036
Tindall JA, Kunkel JR, Anderson DE (1999) Unsaturated water flow in soil. Unsaturated Zo Hydrol Sci Eng (eds Tindall JA, Kunkel JR) 183–199
Wagner FM, Möller M, Schmidt-Hattenberger C et al (2013) Monitoring freshwater salinization in analog transport models by time-lapse electrical resistivity tomography. J Appl Geophys 89:84–95. https://doi.org/10.1016/j.jappgeo.2012.11.013
Wang C, Luo Y, Huo Z et al (2022) Salt accumulation during cropping season in an arid irrigation area with shallow water table depth: a 10-year regional monitoring. Water (switzerland). https://doi.org/10.3390/w14101664
Wirasatriya A, Pribadi R, Iryanthony SB, et al (2022) Mangrove above-ground biomass and carbon stock in the karimunjawa-kemujan islands estimated from unmanned aerial vehicle-imagery. Sustainability 14. https://doi.org/10.3390/su14020706
Yan S, Yu S, Wu Y et al (2015) Seasonal variations in groundwater level and salinity in coastal plain of Eastern China influenced by climate. J Chem. https://doi.org/10.1155/2015/905190
Yoshikai M, Nakamura T, Suwa R et al (2022) Predicting mangrove forest dynamics across a soil salinity gradient using an individual-based vegetation model linked with plant hydraulics. Biogeosciences 19:1813–1832. https://doi.org/10.5194/bg-19-1813-2022

Publisher's Note Springer Nature remains neutral with regard to jurisdictional claims in published maps and institutional affiliations.